2012

Total Variation Based Restoration of Bilevel Waveforms

Rebecca McCarter
Virginia Commonwealth University

TOTAL VARIATION BASED RESTORATION OF BILEVEL WAVEFORMS

A thesis submitted in partial fulfillment of the requirements for the degree of Master of Science at Virginia Commonwealth University.

by

Rebecca Jane McCarter
Master of Science

Director: Dr. Todd Wittman, Assistant Professor
Department of Mathematics and Applied Mathematics

Virginia Commonwealth University
Richmond, Virginia
May 2012

Acknowledgment

The success and completion of this thesis has depended largely on the encouragement and guidance of others. I would like to take this opportunity to express my gratitude towards those individuals.

First and foremost, I would like to thank my thesis adviser, Doctor Todd Wittman, for his patience and willingness to assist me throughout the course of the investigation summarized in this paper. My gratitude extends to the faculty and staff of the Mathematics Department at Virginia Commonwealth University who have provided not only instruction but also mentorship during my undergraduate and graduate endeavors.

I would also like to express my appreciation to my colleagues in the Mathematical Sciences graduate program community. My gratefulness for the support and encouragement provided by my peers cannot be emphasized enough. In particular, I would like to thank Nicole O'Neil, Michelle Grigsby, and Courtney Henry for their constant and unconditional friendship.

Finally, I would like to express my appreciation for the technical and general support provided by my Dear friend Richard.

Contents

List of Figures

Abstract

TOTAL VARIATION BASED RESTORATION OF BILEVEL WAVEFORMS

By Rebecca Jane McCarter, Master of Science.

A thesis submitted in partial fulfillment of the requirements for the degree of Master of Science at Virginia Commonwealth University.

Virginia Commonwealth University, 2012.

Director: Dr. Todd Wittman, Assistant Professor, Department of Mathematics and Applied Mathematics.

A series of Total Variation based algorithms are presented for the restoration of bilevel waveforms from observed signals. The proposed model is discussed analytically and numerically via the gradient descent minimization of the TV energy. The application of restoration of bilevel waveforms encoded within barcode images is presented. A super-resolution technique is proposed as a reduction of dimensionality of the image data. The result is a high resolution image from which the encoded bilevel waveform is restored. Implementation of results is shown for synthetic and real images.

Introduction

Binary signals are prevalent in digital systems and have a wide range of applications including text, data communication packets, and barcodes. A signal is binary if it communicates data by varying between values of zero and one.

Each binary signal can be expressed as a characteristic function of a measurable subset S of the real numbers. That is, the signal takes a value of one on S and a value of zero elsewhere. In this investigation, we will address binary signals as bilevel waveforms. A bilevel waveform over the domain Ω is a function that varies between two possible values.

During the processes of data acquisition, communication, and storage, distortion (blur and noise) is often introduced into the bilevel waveform, compromising the encoded data. This presents a problematic situation in data communication and motivates a series of interesting mathematical queries.

Distortion of the bilevel waveform $u(x)$ will be considered to be the result of blur distortion and additive noise. As in [10], distortion $T_{\alpha,\sigma}$ of the waveform due to blur can be modeled by the convolution of the initial bi-level waveform with a Gaussian kernel G_σ of amplitude α and standard deviation σ denoted by

$$T_{\alpha,\sigma} : u(x) \to \alpha \cdot G_\sigma * u(x)$$

for $\alpha > 0$, and the Gaussian kernel

$$G_\sigma(x) = \frac{1}{\sigma\sqrt{2\pi}} \exp\left(-\frac{x^2}{2\sigma^2}\right) \qquad \text{with } \alpha > 0$$

The incorporation of additive noise $n(x)$ leads to the following hypothesized model for the observed waveform:

$$f(x) = T_{\alpha,\sigma}(u) + n(x)$$

In order to restore the bilevel waveform from the observed waveform $f(x)$, it is necessary to estimate the parameters of the Gaussian kernel. While an attempt to meaningfully execute approximations of these parameters may lead to ill-posed problems for general waveforms, Esedoglu showed that the unique structure of bilevel waveforms will allow effective determination of parameters for small amounts of blur distortion [10].

The current investigation considers variational methods for the restoration of bilevel waveforms from distorted observed signals. Variational methods for noise reduction were first introduced in 1992 by Rudin, Osher, and Fatemi [14], [18]. These methods were originally developed to address two-dimensional data sets such as image data. Since then, there have been numerous extensions and proposed improvements to the methods suggested by Rudin, Osher, and Fatemi. Several extensions include those described in [1], [5], [22], [9], [23]. The detection of edges or discontinuities in the bilevel waveform is a necessary aspect of restoration problems, because the discontinuities explicitly define the binary signal encoded within the waveform. Mumford and Shah are well-known for early work on the problem of edge detection [16]. Extensions of the problem of edge detection can be found in [2], [3], [4]. Preservation of edges in restored waveforms is often compromised by displacement of local extrema within the waveform that is induced by restoration algorithms

developed to reduce blur [21]. This phenomenon is known as convolution distortion. As the standard deviation of the convolution kernel approaches the minimum length of any segment in the bilevel waveform, convolution distortion inhibits the detection of discontinuities in the waveform. An algorithm to account for this issue is addressed by Joseph and Pavlidis [13], [12]. A partially blind deconvolution approach has been shown to more systematically address the problem of convolution distortion [8],[10].

In the present investigation we will discuss, both analytically and numerically, a series of Total Variation (TV) based models for bilevel waveforms adapted from the algorithm proposed by Rudin, Osher, and Fatemi [14]. The modified algorithm minimizes an energy functional by gradient descent and is consequently described by an iterative technique. Although we will discuss numerical implementation, our interest is not the speed but rather the accuracy of the algorithm.

We will also investigate the application of this algorithm to barcode waveforms. Barcode waveforms will be extracted from a super-resolution of image data. This technique incorporates data from the entire barcode image into a single waveform. Both synthetic image and real image data are presented, and numerical techniques for addressing each case are described.

Restoration of a Bilevel Waveform

The current discussion will address several techniques for the restoration of a bilevel waveform $u(x)$ from an observed signal $f(x)$. First, we discuss linear filters and identify inadequacies in these methods. In order to detect and remove artifacts introduced into the waveform by additive noise, it is necessary to consider values of the observed waveform $f(x)$ in a neighborhood about x_0 for each x_0 in the domain Ω. Reduction of noise artifacts may be accomplished by the application of a mean filter. The value of the proposed restored waveform at each value x_0 is given by calculating the mean value of the observed waveform $u(x)$ across a neighborhood about x_0. This is a method of linear smoothing.

Linear smoothing by the application of a mean filter will result in the reduction of noise artifacts but may also introduce additional blur distortion near discontinuities in the ideal bilevel waveform. Restoration attempts by application of a median filter may be less sensitive to the effects of noise artifacts, but a median filter will fail to remove blur distortion. Reduction of noise artifacts is evidenced qualitatively in the mean-filtered and median-filtered waveforms. However, the blur distortion of the observed signal is not improved. Techniques requiring differentiation of the observed waveform in order to calcultate the extrema in the signal and identfy discontinuities in the bilevel waveform are sensitive to noise. The noise artifacts often differ greatly from the nearby values of the waveform and create false extrema. These false extrema are evident in the derivatives of the waveform and lead to inaccurate restoration of the bilevel waveform by inappropriate identification of discontinuities[10]. In the problem of restoring bilevel waveforms, inappropriate definition

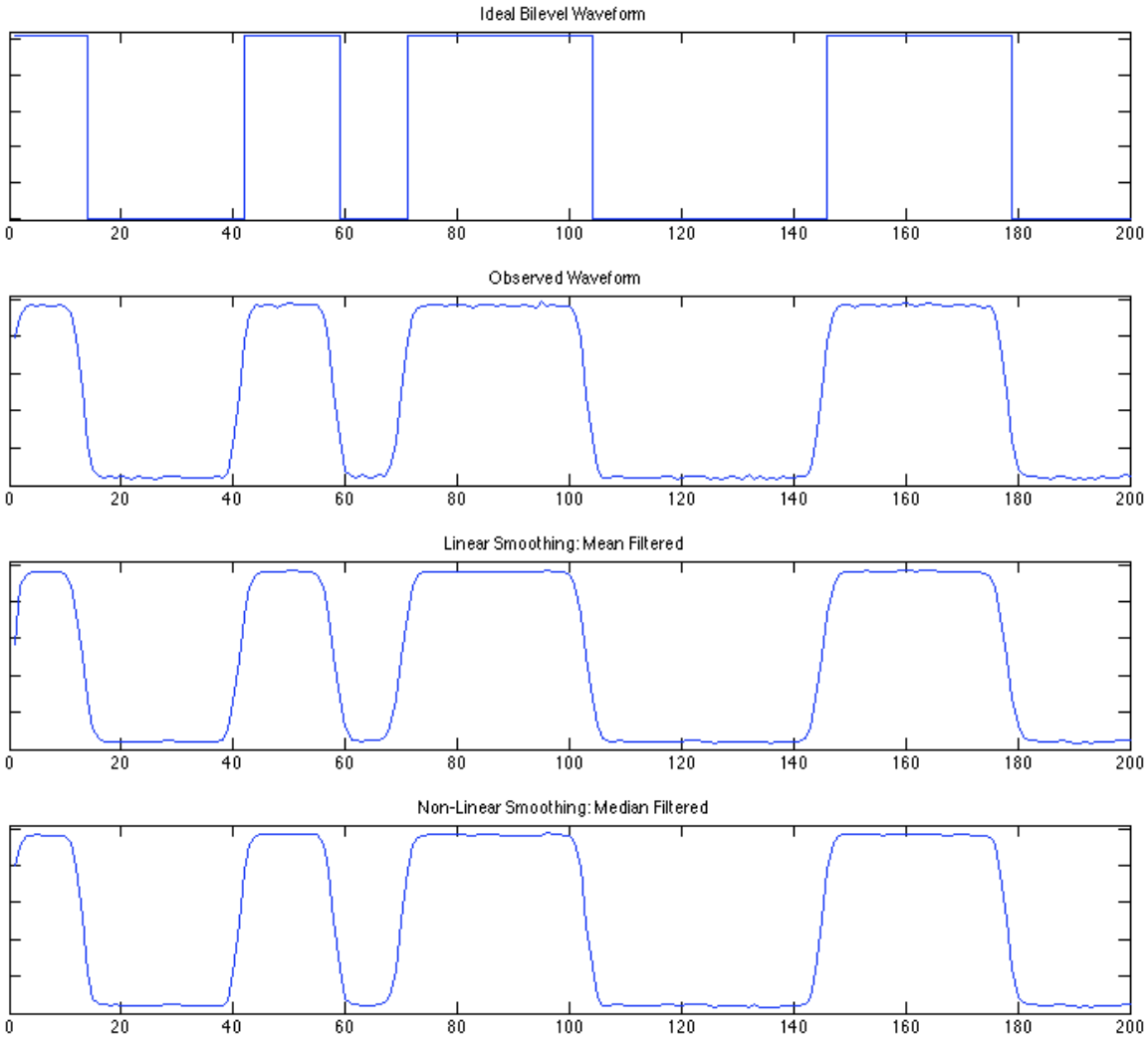

Figure 2.1: Restoration by application of mean and median filters.
From Top to Bottom: Ideal bilevel waveform. Observed distorted signal. Mean-Filtered signal. Median-filtered signal.

of local extrema corresponds to false identification of discontinuities in the binary signal and consequent ineffectiveness of the restoration process.

The first waveform shown in Figure 2.1 displays the ideal bilevel waveform that has been distorted by convolution with a Gaussian kernel and additive noise in the second waveform, as described previously. Noise is evidenced in this waveform by the uneven plateaus that were uniformly values of zero or one in the bilevel waveform. The angled transitions between states within the waveform are the product of blur distortion. The third waveform illustrates the effects of mean filtering. We can see that noise artifcats are reduced in the mean-filtered waveform. The fourth wavefrom The reduction of noise artifacts is not as effective in the fourth waveform. This can be seen easily by observing the values of the waveform between x values of 105 and 140 in the mean-filtered waveform and the median-filtered waveform. It is clear that the mean-filtered waveform is more smooth on this interval than the median-filtered waveform. This corresponds to a more effective reduction of noise by mean-filtering.

2.1 TV Energy Minimization

The values of an observed waveform $f(x)$ can be defined as the energies for each of the x values in the domain Ω. We will define an energy functional for the observed waveform $f(x)$ in order to minimize the first variation of the energy, or the first derivative of the assigned functional, over Ω. The resulting waveform $u(x)$ is the minimizer of the functional and the proposed solution to the restoration problem. We will address three energy minimization algorithms, TV minimization, TV minimization with a penalty function, and a Modica-Mortola approximation to TV minimization.

In order to address the TV Energy minimization of an observed waveform $f(x)$, we note that the observed waveform can be viewed as a function of bounded variation (BV). That is,

the total variation given by

$$TV[f] = \int_{\Omega} |\nabla f|$$

is finite, because $f(x) \in [0,1]$, $\forall x \in \Omega \subset \mathbb{R}$. It is known that for any $f \in BV(\Omega)$, it is possible to find a sequence of approximations (f_n) such that f_n converges to u and $\int_{\Omega} |f_n'| \to \int_{\Omega} |f'|$ as n becomes infinitely large [7]. Thus, $\int_{\Omega} |f_n' - f'| \to 0$ as $n \to \infty$.

We consider a technique for generating an approximation $u(x)$ to a waveform from an observed waveform $f(x)$ based on a variational approach to image processing. We can think of the values of the waveform over the domain Ω as the energy associated with each $x \in \Omega$. In order to reduce the effects of noise and blur, we will assign an energy functional to the waveform that expresses the energy at each $x \in \Omega$. Elimination of distortion within the waveform can be accomplished by minimizing the first variation of energy, or the first derivative of the energy functional. Using a first order optimization algorithm known as gradient descent or method of steepest descent, we find the minimizer of the energy functional over the domain of the waveform. In order to apply this algorithm, we assume that the energy functional is defined and differentiable for all $x \in \Omega$. Then, the function decreases most rapidly in the direction of the negative gradient. Thus, the iterative method of gradient descent steps in the direction of the negative of the gradient of the energy functional for each iteration. The minimizer for the TV energy functional is the proposed solution to the denoising problem.

An approximation $u(x) : \Omega \to \mathbb{R}$ to the original waveform can be recovered from the observed signal $f(x)$ by minimizing the TV energy proposed by Rudin, Osher, and Fatemi [14]. The TV energy functional of a waveform can be expressed as

$$E[u \mid f] = \int_{\Omega} |u_x| \, \mathrm{d}x + \lambda \int_{\Omega} (u-f)^2 \, \mathrm{d}x$$

where the domain of integration $\Omega \subset \mathbb{R}$ is the domain of the observed waveform and is restricted to the real-line, $\lambda \geq 0$ is a Lagrange multiplier, and $u(x) : \Omega \to \mathbb{R}$. The energy is written as a function of a guess for the improved signal u given the observed waveform f. The first term gives the Total Variation of the current approximation and the second term is a fidelity term, relating the approximation to the observed waveform. In practice, we take the observed waveform f to be the initial guess for the restored waveform u. The minimizer of this functional over the given domain is the proposed solution.

It is known that, for an observed waveform $f \in L^1(\Omega)$, the minimizer of the TV energy in $BV(\Omega)$ exists and is unique [7].

Although we restrict the domain to the real line, it is straightforward to extend this technique to higher dimensions.

We are interested in the minima of this functional, so we will consider the stationary points. In order to determine the functions for which a given functional is stationary, we evaluate the Euler- Lagrange equation for the functional. The Euler-Lagrange equation for a functional $E[u] = g(x, u_x)$ is

$$\nabla E = -\frac{\partial}{\partial x}\frac{\partial g}{\partial u_x} + \frac{\partial g}{\partial u}$$

In this case, our functional is

$$g(x, u_x) = |u_x| + \lambda (u-f)^2$$

so we have

$$\nabla E = -\frac{\partial}{\partial x}\mathrm{sign}(u_x) + 2\lambda (u-f)$$

The sign function is discontinuous at $u_x = 0$, so the Euler-Lagrange equation is numerically unstable when $u(x)$ is constant in x. For a binary signal $u(x)$, $u_x = 0$ for all $x \in \Omega$ except those x at which the bilevel waveform is discontinuous. Thus, the Euler-Lagrange equation for this functional cannot be differentiated with respect to x. We numerically approximate the sign function. In order to construct a numerical approximation, we will use the following continuous approximation for the sign function:

$$\text{sign}(u_x) \cong \frac{2}{\pi} \arctan\left(\frac{u_x}{\varepsilon}\right)$$

for small positive values of the parameter ε. In application, it is necessary to maintain values of ε sufficiently large to avoid numerical instability of the approximation as ε approaches zero.

Therefore, we approximate the Euler-Lagrange equation by

$$\nabla E \cong -\frac{2}{\pi} \varepsilon u_{xx} \left(\varepsilon^2 + u_x^2\right)^{-1} - 2\lambda (u - f)$$

which motivates the following approximation to the gradient descent of the TV energy

$$\frac{\partial u}{\partial t} \cong \frac{2}{\pi} \varepsilon u_{xx} \left(\varepsilon^2 + u_x^2\right)^{-1} - 2\lambda (u - f)$$

Numerically, the gradient descent is discretized by a forward Euler method as

$$u^{n+1} = u^n + \Delta t \left[\frac{2}{\pi} \varepsilon u_{xx}^n \left(\varepsilon^2 + (u_x^n)^2\right)^{-1} - 2\lambda (u^n - f)\right]$$

where Δt is the time step, f is the observed waveform, and u^n is the n^{th} iterate. The first and second derivatives of $u(x)$with respect to x are calculated by finite difference schemes. For applications requiring larger values of Δt, an implicit scheme would be faster than the proposed method and stable.

The minimizer of this functional exists on a bounded domain, and a solution consequently exists for the energy function described here. Esedoglu shows that for sufficiently large values of λ, a generalized form of this technique is effective in recovering the original signal $u(x)$ [10].

Esedoglu also describes an approach for the reduction of blur in the observed waveform [10]. In [10], Esedoglu presents an algorithm for partially blind deconvolution of barcode signals. Although we focus mainly on the reduction of noise in the observed waveform in the present investigation, the partially blind deconvolution approach to blur reduction taken by Esedoglu should be considered when addressing the general restoration problem.

In order to account for blur in the observed waveform, we incorporate the Gaussian Kernel G_σ of unknown amplitude α and standard deviation σ given by

$$G_\sigma(x) = \frac{1}{\sigma\sqrt{2\pi}} \exp\left(-\frac{x^2}{2\sigma^2}\right), \qquad \text{with } \sigma > 0,$$

and introduce the following energy functional

$$E[u] = \int_\Omega |u_x| \, dx + \lambda \int_\Omega (\alpha G_\sigma * u - f)^2 \, dx + \beta \int_\Omega u^2 (1-u)^2 \, dx$$

This energy functional follows the form of the TV energy proposed by Rudin, Osher, and Fatemi [14]. However, noise reduction is incorporated into the functional by convolution of the proposed solution u with the Gaussian kernel. The addition of the third term serves as a penalty function, forcing the values of the recovered signal to approach zero and one. This term is useful in the restoration of a binary-valued waveforms. In [10] Esedoglu shows that for small amounts of blur, the proposed method is well-defined. Meaningful approximations for the unknown parameters of the Gaussian kernel can be calculated systematically, and the minimizer of this energy functional over the initial guess for the solution is an approximation

to the desired waveform [8].

Figure 2.2 illustrates the effects of applying TV energy minimization to a noisy observed waveform. The first graph shows the ideal bilevel waveform. In the third graph, the TV denoised waveform exhibits a reduction in noise artifacts. However, the discontinuities in the bilevel waveform are represented by smooth curves and binary values are not obtained. Additional improvements can be made to the resulting waveform in order to restore the bilevel waveform.

2.2 TV Energy Minimization of a Bilevel Waveform

The TV energy minimization scheme discussed in the previous section can be modified for the restoration of bilevel waveforms. Bilevel waveforms are unique in that they take values of only zero and one. We adapt the general one-dimensional TV energy minimization technique to the bilevel waveform restoration problem by adding a penalty term to the TV energy function. This term forces the proposed restoration $u(x)$ to take values of zero or one. Addition of this term is unique to the problem being addressed, since values of the ideal waveform are binary. Figure 2.2 gives a qualitative illustration of the improvement achieved by addition of a penalty term. The third curve shows the results of TV minimization denoising, and the fourth curve shows the effects of adding a penalty function to this method. In the fourth curve, it is clear that the peaks of the waveform are flattened and forced towards values of zero and one.

We will use the 'double-well function' $W(u) = u^2(1-u)^2$as the penalty term. The function $W(u)$ has minima at $u = 0$ and $u = 1$, so addition of this term will force values of the waveform to approach 0 and 1. The TV energy is given by

$$E[u] = \int_{\Omega} |\nabla u| + \lambda \int_{\Omega} (u-f)^2 + \beta \int_{\Omega} W(u)$$

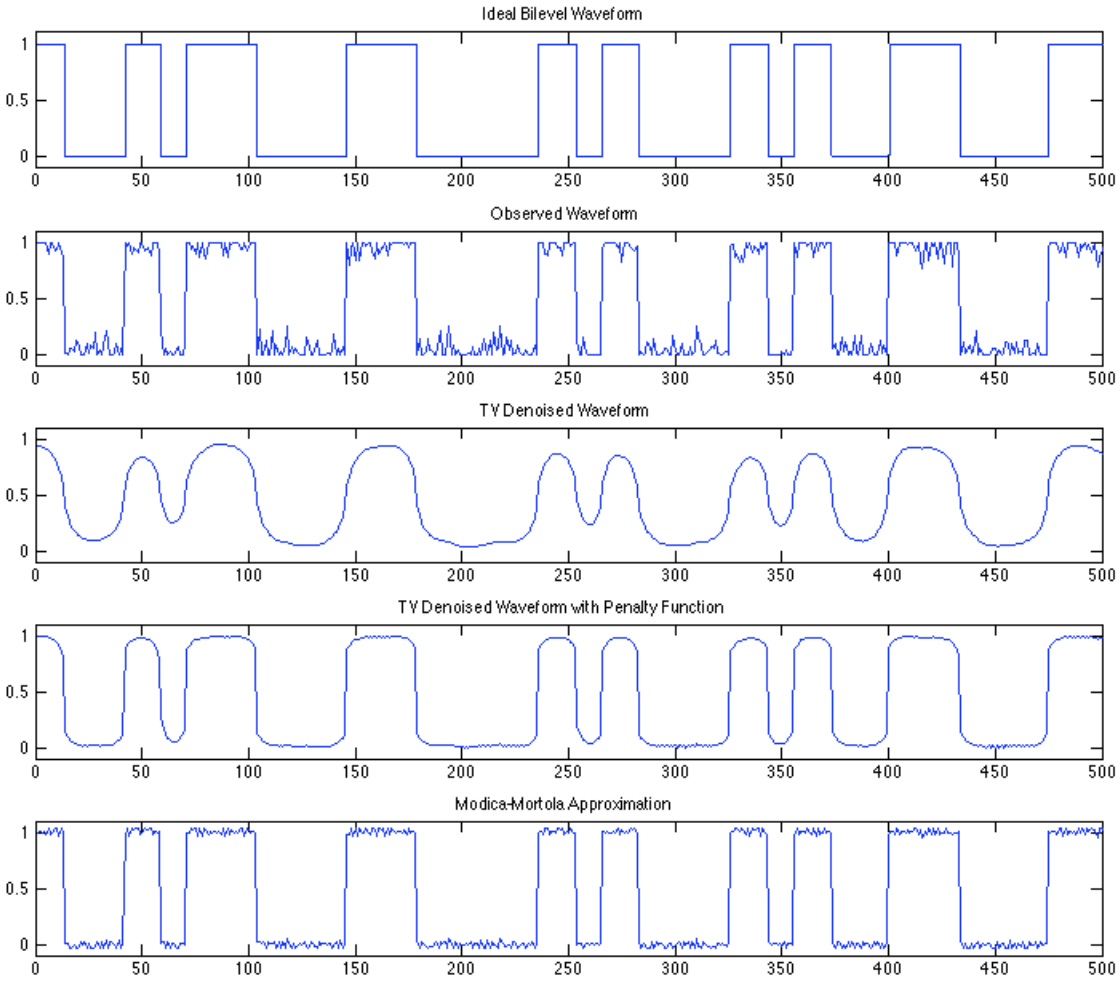

Figure 2.2: Variational Methods
From top to bottom: Ideal bilevel waveform, observed waveform, TV denoised waveform, TV denoised waveform with penalty function, Modica-Mortola approximation waveform.

for strictly positive values of β.

Esedoglu shows in [10] that the with addition of the 'double-well' function, the new problem is well-posed. Minimizers over the domain of the observed waveform are proposed restorations of the bilevel waveform.

The new Euler Lagrange equation is given by

$$\nabla E \cong -\frac{2}{\pi}\varepsilon u_{xx}\left(\varepsilon^2+u_x^2\right)^{-1}+2\lambda\left(u-f\right)+\beta\left(2u-6u^2+4u^3\right)$$

The Euler-Lagrange equation is derived by the same process described before. We have modified the energy functional of the previous section by the addition of the penalty term. This new term does not contain x derivatives of u. Therefore, our new Euler-Lagrange equation differs from the functional of the last section only by the addition of the of the u derivative of the penalty function. Minimization by gradient descent implies that

$$\frac{\partial u}{\partial t} \cong \frac{2}{\pi}\varepsilon_{xx}\left(\varepsilon^2+u_x^2\right)^{-1}-2\lambda\left(u-f\right)-\beta\left(2u-6u^2+4u^3\right)$$

and this equation is numerically discretized as

$$u^{n+1}=u^n+\Delta t\left[\frac{2}{\pi}\varepsilon u_{xx}^n\left(\varepsilon^2+(u_x^n)^2\right)^{-1}-2\lambda\left(u^n-f\right)-\beta\left(2u^n-6\left(u^n\right)^2+4\left(u^n\right)^3\right)\right]$$

2.3 Modica-Mortola Approximation

The restoration algorithms described previously can be approximated by considering the minimizer of a related functional. We use the results of Modica and Mortola to describe such an approximation. Minimization of the TV energy of the observed waveform $f(x)$ over the proposed restored waveform $u(x)$, $\underset{u(x)}{min}E\left[u \mid f\right]$ is approximated in previous sections by substitution of the numerical approximation $\operatorname{sign}(u_x) \cong \frac{2}{\pi}\arctan\left(\frac{u_x}{\varepsilon}\right)$.

However, an exact calculation of the proposed restoration can be obtained by applying the results of Modica and Mortola [15]. We write a functional E_δ for which the minimizer is equal to the minimizer of the proposed TV energy functional

$$\min_{u(x)} E\left[u \mid f\right] = \min_{u(x)} E_\delta\left[u \mid f\right]$$

Based on the results of Modica and Mortola, we consider the minimizer of following energy over the entire waveform

$$E_\delta\left[u \mid f\right] = \int_\Omega \left(\delta\left(u_x\right)^2 + \frac{1}{\delta} W\left(u\right)\right) + \lambda \int_\Omega \left(u-f\right)^2$$

for small positive values of the parameter δ, and $\mathrm{W}(u) = u^2(1-u)^2$ is the penalty function described in the previous section.

For a one-dimensional waveform, we consider the energy

$$E_\delta\left[u \mid f\right] = \int_{\Omega\subset\mathbb{R}} \left(\delta\left(u_x\right)^2 + \frac{1}{\delta}\left(u^2(1-u)^2\right) + \lambda\left(u-f\right)^2\right) dx$$

We will address the minimization of the proposed energy functional by gradient descent. The Euler-Lagrange equation ∇E_δ for the energy functional E_δ is given by

$$\nabla E_\delta = -2\delta u_{xx} + \frac{1}{\delta}\left(2u - 6u^2 + 4u^3\right) + 2\lambda\left(u-f\right)$$

and minimization by gradient descent gives

$$\frac{\partial u}{\partial t} = 2\delta u_{xx} - \frac{1}{\delta}\left(2u - 6u^2 + 4u^3\right) - 2\lambda\left(u-f\right)$$

This equation is numerically discretized as

$$u^{n+1} = u^n + \Delta t \left[2\delta u_{xx}^n - \frac{1}{\delta} \left(2u^n - (6u^n) + (4u^n)^3 \right) - 2\lambda \left(u^n - f \right) \right]$$

This method incorporates the binary value constraint on the restored waveform by the implementation of a penalty function. The method allows us to observe an exact calculation of the gradient descent by application of the findings of Modica and Mortola, since we have eliminated the numerical approximation of the sign function. It is known that this problem has a unique solution and the minimizer is attained [10].

A qualitative comparison of the technique justified by the results of Modica and Mortola can be seen in Figure 2.2. The Modica-Mortola algorithm shows a significant improvement in the restoration of the binary values evident in the bilevel waveform.

Super-Resolution of Bilevel Waveforms from Barcode Images

3.1 Barcode Images

There are a wide range of applications for the algorithms presented. In this discussion, applications to barcodes are addressed. A super-resolution technique for barcode images is presented and approached as a reduction of the dimensionality of the image.

Barcode images are a two-dimensional method for storage and communication of binary data. They are composed of a series of alternating bars and spaces of varying width. Information is encoded using the pattern and widths of individual bars and spaces. The width of each bar is an integer multiple of the width of a unit bar contained within the image. The unit bar provides a scale factor for decoding and a series of checks to ensure that appropriate data is extracted from the image. The distribution of unit bars within each barcode serves as a check for the proper decoding of the barcode image.

Encoded information is traditionally extracted using laser scanners to observe a one-dimensional subset of the barcode image. We refer to the observed one-dimensional subset as a scanline. A scanline is interpreted by decoding software, and the remainder of the image is not used to recover the encoded information. In the event that an observed scanline is corrupted, incomplete, or is unable to be decoded by decoding software, the scanner will observe and consider another scanline. This approach to barcode decoding is effective in industry because of the high-resolution signal obtained by using a laser scanner.

However, data acquisition techniques that obtain a two-dimensional image of the barcode require imaging scanners that can simultaneously observe the information in the entire image

Figure 3.1: Ideal barcode image.

such as digital cameras. While laser scanners acquire signals of higher resolution than digital cameras, they are ineffective in two-dimensional imaging of barcodes. Decoding applications on mobile devices such as smart phones present an interesting application for extraction and decoding of bilevel waveforms from barcode image data. Limited resolution, distortion, and additive noise associated with the acquisition and storage of image data using mobile devices often prevents the effective extraction of a decodable waveform. Noise and blur distortion in the barcode image of Figure **??** prevent decoding using a single scanline from the image data and current decoding algorithms.

Barcode images $u(x,y)$ that we consider are pixelated representations of an ideal barcode. We address each ideal barcode as a two-dimensional array of binary data such that for all pixels (x,y), the value stored in the array is an element of $\{0,1\}$. Figure 3.1 shows an ideal barcode image in which each element of the array is binary valued. With the introduction of distortion, noise, and blur, we will see that the values of the array become elements of the closed interval $[0,1]$. Distortion compromises the integrity of the barcode image and may prevent decoding. Figure 3.2 shows distortion of a pixelated barcode image. The image clearly shows noise artifacts in the white spaces of a rotated barcode. Noise artifacts can be identified by single pixels that are dramatically different in value than those surrounding them. In the image, there are also pixels taking values other than black and white along the edges of the bars. This is evidence of blur distortion.

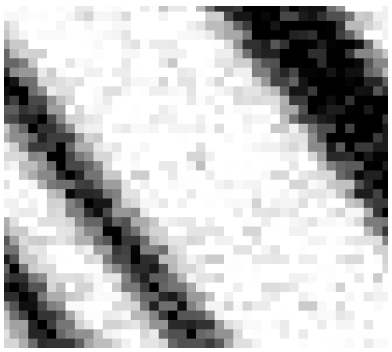

Figure 3.2: Blur and noise in pixelated barcode image.

3.2 Super-Resolution Schemes

In order to restore a binary sequence and the corresponding bilevel waveform, we will consider a super-resolution of the image data. While traditional methods of barcode decoding consider only a single scanline, a super-resolution scheme incorporates the information contained in each of the scanlines to form a single waveform.

Super-resolution is a technique used frequently in medical imaging, satellite imaging, and video applications to construct a single high-resolution (HR) image from a series of low-resolution (LR) images [19]. Two successive processes are generally used to generate the HR image. The first process involves the alignment of images, as it is likely that the data contained in each image is not spatially aligned within the frame. Fusion of the images is the second process. The images must be meaningfully combined to form a single HR image [11].

We adapt the concept of super-resolution to a reduction in dimensionality of barcode images. A two-dimensional barcode image can be expressed as an array of individual scanlines. We align and fuse the individual scanlines to form a single HR waveform that is representative of the entire LR barcode image. The waveforms extracted from barcode images are one-dimensional data sets, so we eliminate the need for repeated sampling of the image [6].

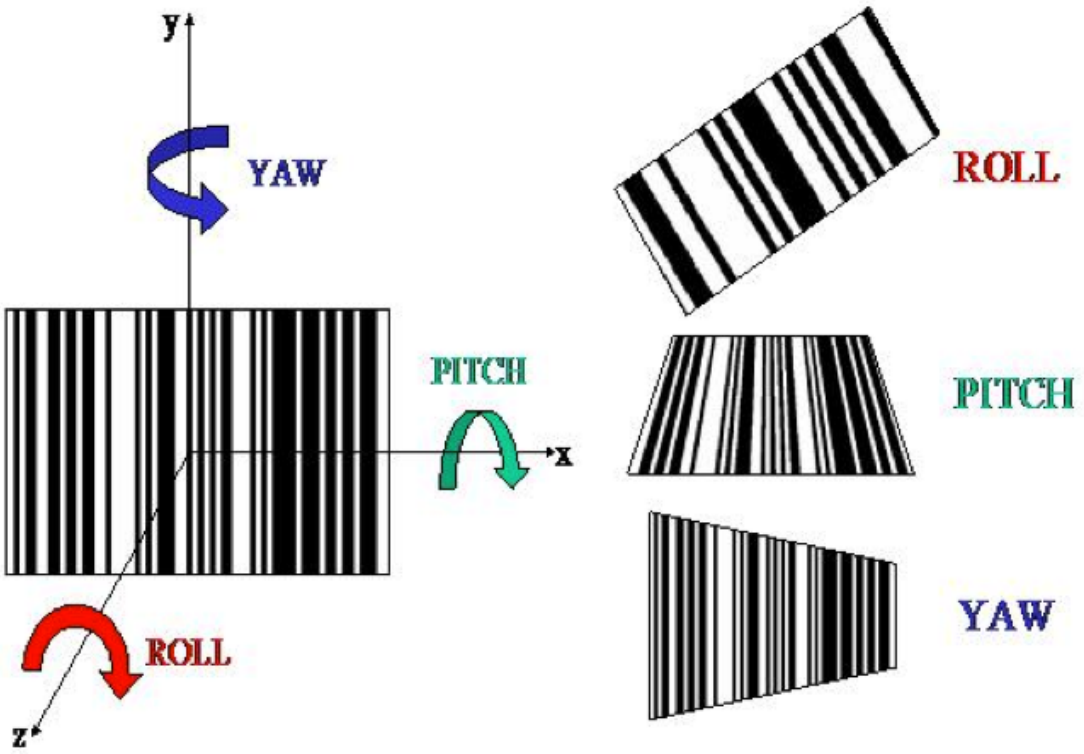

Figure 3.3: Three degrees of freedom in barcode rotation. [24]

In addition to blur and noise, barcode images virtually always contain geometric sampling distortion. When the picturing plane and the plane containing the original barcode are not parallel, geometric sampling distortion will be evident in the acquired barcode image. By exploiting the sampling distortion, geometry, and high contrast of barcode images, we are able to compose schemes for super-resolution of image data to form a HR waveform. We address three cases of sampling distortion (Figure 3.3).

We assume that the original barcode is printed on a planar surface and consider three mechanisms of rotation relative to the picturing plane of the camera. The case of no rotation is addressed as a trivial case. Virtually all barcode images exhibit geometric sampling distortion. The yaw case is achieved when the distance between the plane containing the original image and the camera lens is not horizontally uniform. The pitch case results from

Figure 3.4: Synthetic no rotation barcode image
From top to bottom: No rotation barcode image and mean filtered projected waveform.

vertical displacement non-uniformity between the lens and image plane and occurs when the top or bottom of the barcode is brought closer to the camera. The roll case refers to rotation of the barcode image within the plane. For each case, we present a super-resolution scheme for extracting a single HR waveform from all of the data contained in the barcode image.

3.2.1 Case 1: No Rotation and the Yaw Case

The case of no rotation is a trivial case. In practice, we expect to have barcode images with either or both of pitch and roll distortion. We create a single waveform from the trivial barcode image by projecting the data from each pixel of the barcode image onto a projection axis t that is perpendicular to the bars of the barcode. Note that this construction produces degenerate sampling of the image: the same point along the projection line represents each pixel in the corresponding pixel column of the barcode image.

We alleviate this problem by applying a mean filter to the data in each pixel row of the barcode image in order to calculate the corresponding value within our projected waveform.

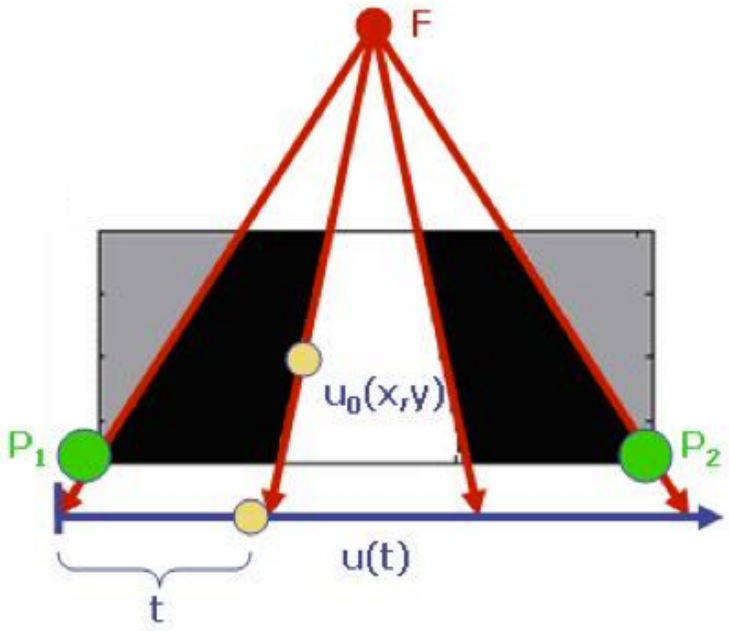

Figure 3.5: Pitch case projection schematic [24]

Figure 3.4 shows a barcode image and the corresponding waveform generated by applying a mean filter to the image. In the no rotation case, the reduction of noise artifacts and local obstruction or distortion of the barcode image can be restored by mean filtering of the array columns.

We restore the bilevel waveform encoded in the barcode data by applying the techniques discussed in the previous chapter with $\Delta t = 1$, since each value in the waveform represents the mean of a column of pixelated values.

We address the yaw case in the same fashion. Since the distortion in the yaw case is only of the relative widths of the bars within the barcode, we apply a mean filter to the acquired barcode image and leave the interpretation of relative widths of bars to the decoder.

3.2.2 Case 2: The Pitch Case

In the pitch case, the bars will not appear to be parallel in the barcode image. Based on perspective geometry, the bars should converge to a focal point $F = (x_F, y_F)$ that we extrapolate from the data contained in the barcode image. The location of the focal point can be calculated by a least-squares method [24]. A schematic describing the projection method is shown in figure 3.5. Each pixel in the barcode image $u_0(x_0, y_0)$ is traced along a vector connecting F to the point (x_0, y_0) and projected onto the projection axis t (Figure 3.5). The resulting HR waveform is $u(t)$. This method for super-resolution by dimension reduction is explained in depth in [24].

3.2.3 Case 3: The Roll Case

Image acquisition and storage in the roll case creates additional blur distortion, as the image is discretized into pixels at an angle different than that of the orientation of the bars of the barcode. The blur distortion and noise introduced by pixelating a barcode image is illustrated in Figure 3.2. As in the case of no rotation and yaw, we will project the data contained in each pixel to a point along a projection axis t that is perpendicular to the orientation of the bars within the barcode.

Based on the work of Safran and Oktem, we assume that the angle of rotation within the plane can be determined by an application of edge detection algorithms [20]. One such algorithm is based on the Hough transform. The Hough transform is an image processing technigue used to detect lines within an image. Detection of the lines along the edges of bars in the barcode image enables the extraction of the rotation angle for real images.

We derive a super-resolution scheme to project each pixel value in the image array onto a projection axis t. The projected data will compose a HR waveform. Figure 3.6 illustrates the schematic used to derive the trigonometric projection of the data value corresponding to

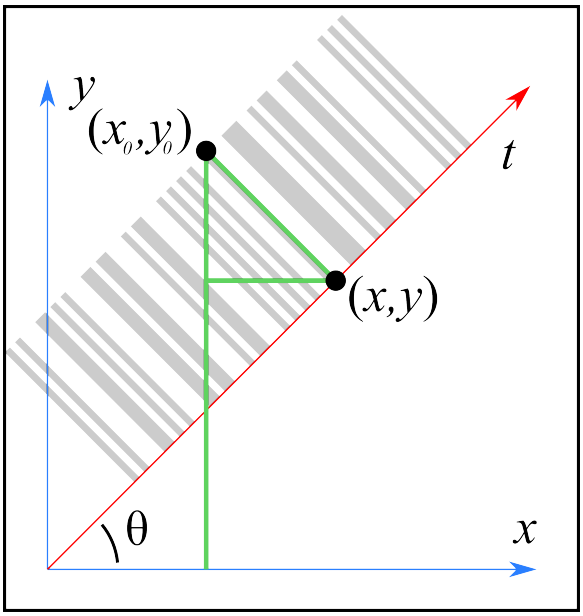

Figure 3.6: Roll case projection schematic.

each pixel within the image array to a point along the projection axis. For a pixel (x_0, y_0) in the original image array, the corresponding ordered pair along the projection axis (x, y) is given by:

$$x(x_0, y_0, \theta) = x_0 + \sin\theta\cos\theta\,(y_0 - x_0\tan\theta)$$
$$y(x_0, y_0, \theta) = x_0\cos\theta\sin\theta - y_0\sin^2\theta$$

where θ is the angle of rotation within the picture plane.

The resulting waveform $P(x) : X \to u_0(x_0, y_0)$ is expressed as a vector of x-coordinates X along the projection axis t and the corresponding vector of pixel values $u_0(x_0, y_0)$ projected from the barcode image array u_0.

Theorem. *The roll case projection given by*

$$x(x_0, y_0, \theta) = x_0 + \sin\theta\cos\theta\,(y_0 - x_0\tan\theta)$$
$$y(x_0, y_0, \theta) = x_0\cos\theta\sin\theta - y_0\sin^2\theta$$

yields degenerate sampling if and only if the $\tan(\theta)$ *is rational.*

Proof. Assume that two pixels (x_0, y_0) and $\left(x_0', y_0'\right)$ map to the same x-coordinate along the projection axis. Then $x = x'$ under the mapping $x(x_0, y_0, \theta) = x_0 + \sin\theta\cos\theta(y_0 - x_0\tan\theta)$. Equivalently, $x_0 + \sin\theta\cos\theta\,(y_0 - x_0\tan\theta) = x_0' + \sin\theta\cos\theta\left(y_0' - x_0'\tan\theta\right)$. By algebra and trigonometric identities,

$$\left(x_0 - x_0'\right)\left(1 - \sin^2\theta\right) = \left(y_0' - y_0\right)\sin\theta\cos\theta \Rightarrow \frac{\sin\theta\cos\theta}{\cos^2\theta} = tan(\theta) = \frac{\left(x_0 - x_0'\right)}{\left(y_0' - y_0\right)}$$

Since the coordinates x_0, y_0, x_0' and y_0' are non-zero natural numbers, the tangent of the angle of rotation θ must be rational in order for degenerate sampling to occur. □

In the no rotation case, the x coordinates of the projected waveform were evenly spaced along the projection axis. Each x in the projected waveform corresponded to one column of pixels within the image array. However, the projected waveform in the current case is determined by a trigonometric projection scheme. Consequently, the distance between data points in the HR projected waveform is not constant. Although the waveform $P(x)$ is non-uniform spatially, in the absence of noise artifacts, it is possible to restore the bilevel waveform encoded within the barcode directly.

In previous cases, we reduce the effects of noise artifacts by application of a mean filter. In the roll case, our projection signal assigns a unique x-coordinate to each pixel in the barcode image array in order to create the super-resolution projection waveform $P(x)$. Noise artifacts introduce dramatic increases in the gradient of the projected waveform $P(x)$. Consequently, variational methods may not distinguish between noise artifacts in the projected waveform $P(x)$ and discontinuities in the ideal bilevel waveform corresponding to the edges of bars in the original barcode image.

We consider several methods for the interpolation of a uniformly spaced super-resolution waveform $H(x_0)$ from the projection waveform $P(x) : X \to u_0(x_0, y_0)$. Each value in the new waveform $H(x_0)$ can be calculated by a Gaussian weighted average. For each x_0 in the interpolated uniformly-spaced projection signal $H(x_0)$, we calculate the value of $H(x_0)$ by considering a weighted average of the points in a neighborhood about x_0 in $P(x)$. The weights assigned to each data point in the neighborhood about x_0 in $P(x)$ are given by a Gaussian distribution centered at the point x_0. We select a uniform step size $\Delta x < 1$ pixel and assign new x-coordinates to the waveform $H(x_0)$ by $x_0 = n\Delta x$ where $n = \frac{[\max(X) - \min(X)]}{\Delta x}$. We may also consdier a nearest neighbor interpolation to create a uniform signal. However, a nearest-neighbor interpolation for $H(x_0)$ will not eliminate the effects of noise artifacts in all cases.

The resulting spatially uniform interpolated waveform $H(x_0)$ is used to restore the encoded bilevel waveform of the barcode by variational methods discussed in Chapter 2.

Numerical Results

The TV energy minimization and Modica-Mortola discretized gradient descent schemes were implemented using MATLAB©. We applied the numerical techniques described in the previous chapter to a number of synthetic and real barcode images.

4.1 Synthetic No Rotation Case

Reduction of dimensionality in the case of no rotation does not produce a HR signal. The case of no rotation is illustrated in Figure 4.1. The barcode image is distorted by the addition of Gaussian noise, and a single scanline is not able to decode due to the presence of noise artifacts in each scanline. The second plot in Figure 4.1 shows the waveform associated with a single extracted scanline from the image. Comparing this to the bilevel waveform encoded within the barcode, as shown in the first plot, it is evident that the presence of noise within the image his distorted the scanline. The third plot shows the mean-filtered waveform. The mean-filtered waveform contains the same amount of information present in a single scanline. However, the mean-filter has reduced the effects of individual noise artifacts throughout the image enough to restore the discontinuities within the original bilevel waveform. The fourth waveform illustrates the effects of the TV denoising algorithm. The peaks appear to be smooth, but the binary values of the bilevel waveform are not restored. The addition of a penalty function forces values in this waveform towards zero and one, as evidenced in the fifth plot. The sixth plot shows the restored waveform produced by the Modica-Mortola scheme. The binary values and definition of discontinuities have been

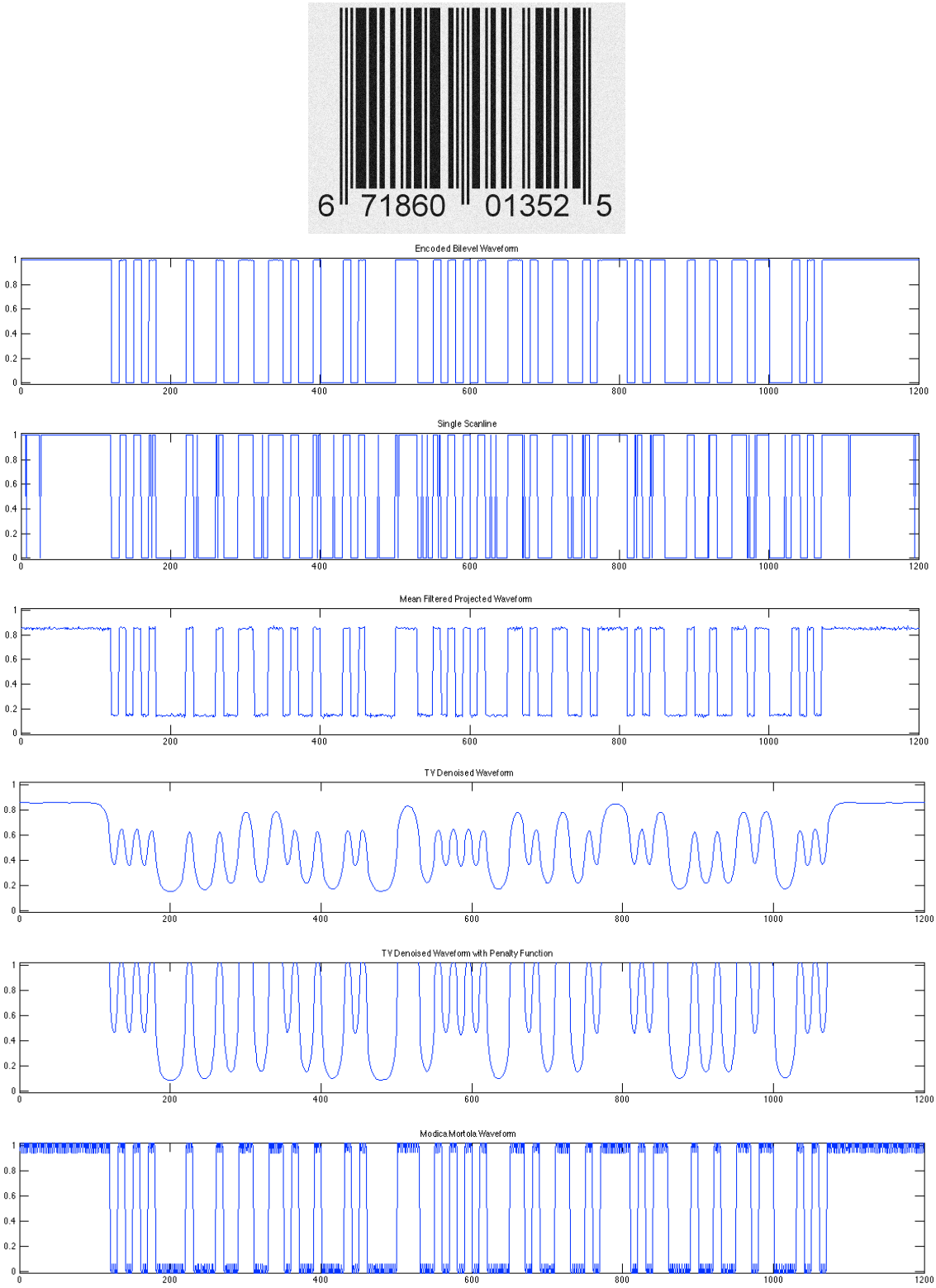

Figure 4.1: Synthetic Case 1: No rotation.
From top to bottom: Barcode image, encoded bilevel waveform, 17th scanline waveform, mean filtered projection, TV denoised projection waveform, TV denoised projection waveform with penalty function, Modica Mortola Waveform. $(T = 20, \delta = \beta = \lambda = 0.1)$

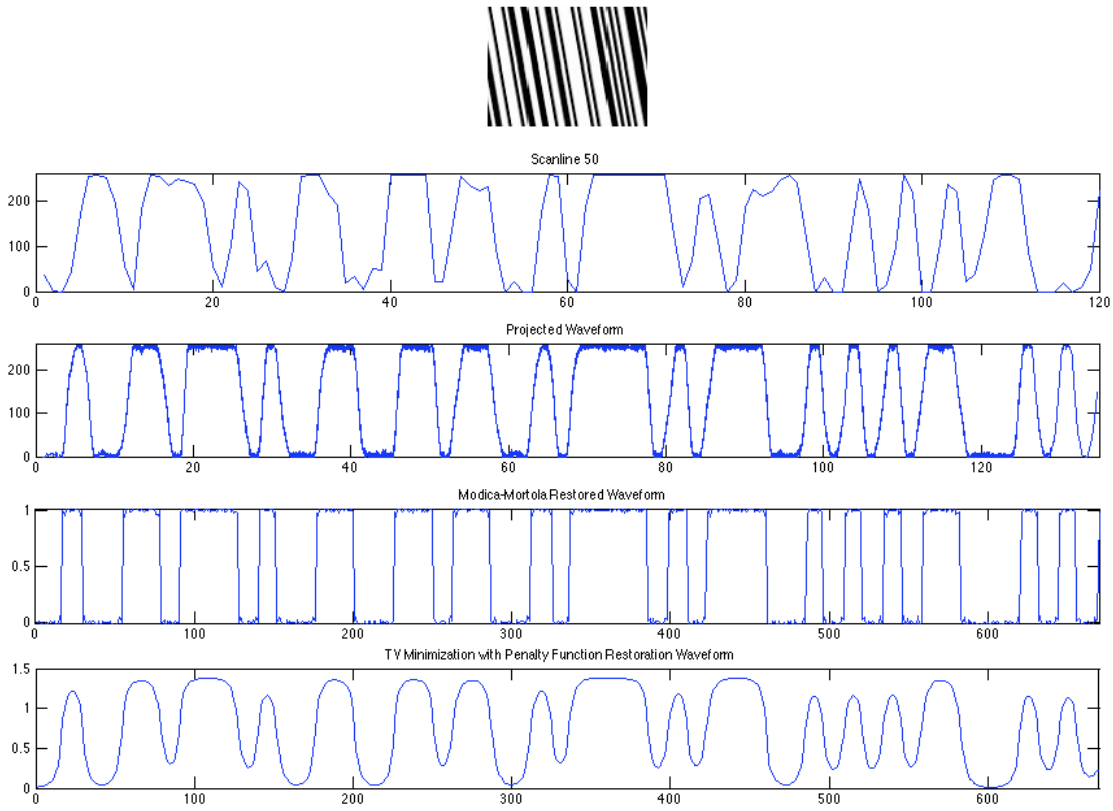

Figure 4.2: Synthetic Roll Case
From top to bottom: Single Scanline, HR Projected Waveform, Modica-Mortola Restored Waveform($T = 5, \delta = \beta = \lambda = 0.1$), TV Restored Waveform ($T = 20, \delta = \beta = \lambda = 0.1$)

restored. This is due to the fact that the Modica-Mortola approximation of the TV energy defines a diffuse interface problem.

4.2 Synthetic Roll Case

Super-resolution by dimension reduction in the rotation case produces a HR projection waveform. In Figure 4.2 a synthetic barcode image is presented. The synthetic rotation of the barcode ten degrees introduced blur into the image. The first plot in Figure 4.2 illustrates the waveform corresponding to a single scanline of the image data. Blur distortion is evidenced

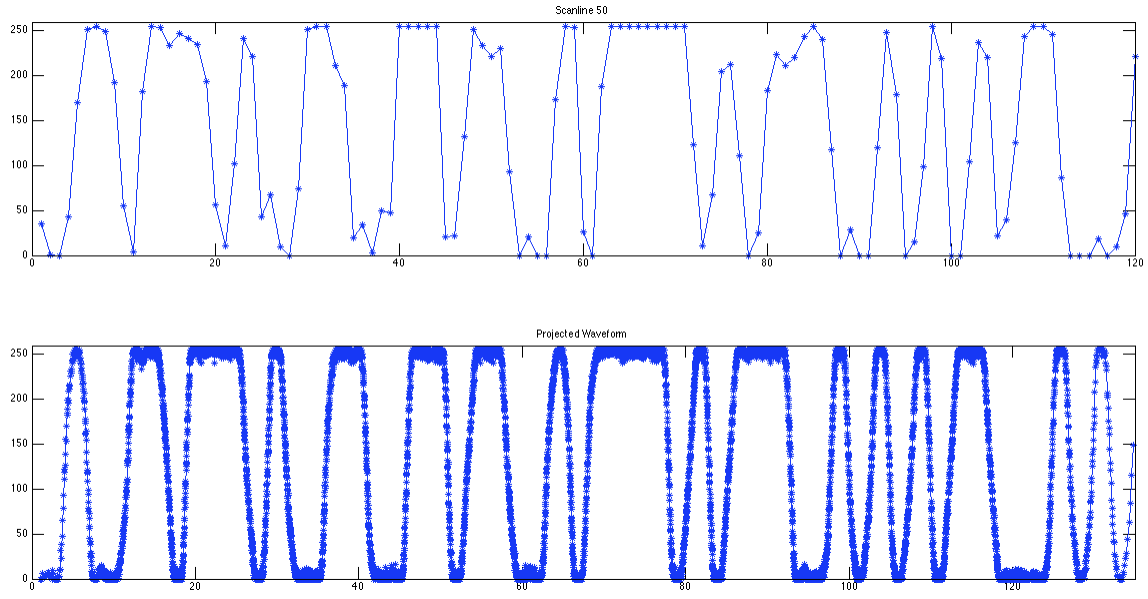

Figure 4.3: Data Density in Synthetic Roll Case
From top to bottom: Data distribution from single scanline, Data distribution from projected waveform

by the curvilinear peaks of the waveform. The trigonometric scheme described previously was applied to generate the projected HR waveform shown in the second plot.

Figure 4.3 shows the increased resolution of the projected waveform. The first plot shows a section of the single scanline extracted from the rotated image. Each asterisk represents a data point defining the waveform. The second figure shows a corresponding section of the projected waveform. Again, each asterisk represents a data point defining the waveform. It is evident that there are substantially more data points within the HR projected signal. The increased resolution of the signal is a consequence of projecting all of the data contained in the barcode image along a single axis and is beneficial in the elimination of distortion within the image. We will see in later results that the constructon of a HR projected signal may help to recover data that is lost in each scanline throughout the entire image.

The third plot in Figure 4.2 illustrates the waveform restored by the Modica-Mortola scheme. Binary values are recovered and discontinuities are consistent with the encoded

bilevel waveform. The fourth plot displays the results of the TV minimization with penalty function scheme. Though noise artifacts have been reduced, blur is still evident in the waveform and the penalty function has not effectively forced values of zero within the waveform.

4.3 Real Rotation

A real rotation image and the corresponing waveforms are shown in Figure 4.4. The image shown was photographed using the camera on a smartphone and cropped to analyze only a portion of the image data. The first plot shows the waveform corresponding to a single scanline. Both blur and substantial noise distortion are illustrated in the scanline waveform. The high resolution projected signal shown in the second plot contains information from the entire image. Consequently, the effects of noise evidenced in the single scanline have been lessened. For example, inconsistencies in the heights of the peaks in the waveform are not as great as those seen in the waveform representing the single scanline. In this case, both the TV with penalty function scheme, in plot three, and the Modica-Mortola scheme, in plot four, effectively recover each of the bars as well as the binary values of the waveform. The lenth of the scanlines in both the Modica-Mortola and TV restorations is noteworthy. They are on the order of 100 times the length of the single scanline waveform, and they contain substantially more data than the single scanline. The HR waveform enabled by the presence of roll distortion also enables the recovery of binary values by the TV scheme, a result that was not seen for the no rotation case in which the development of a super-resolution signal was not possible.

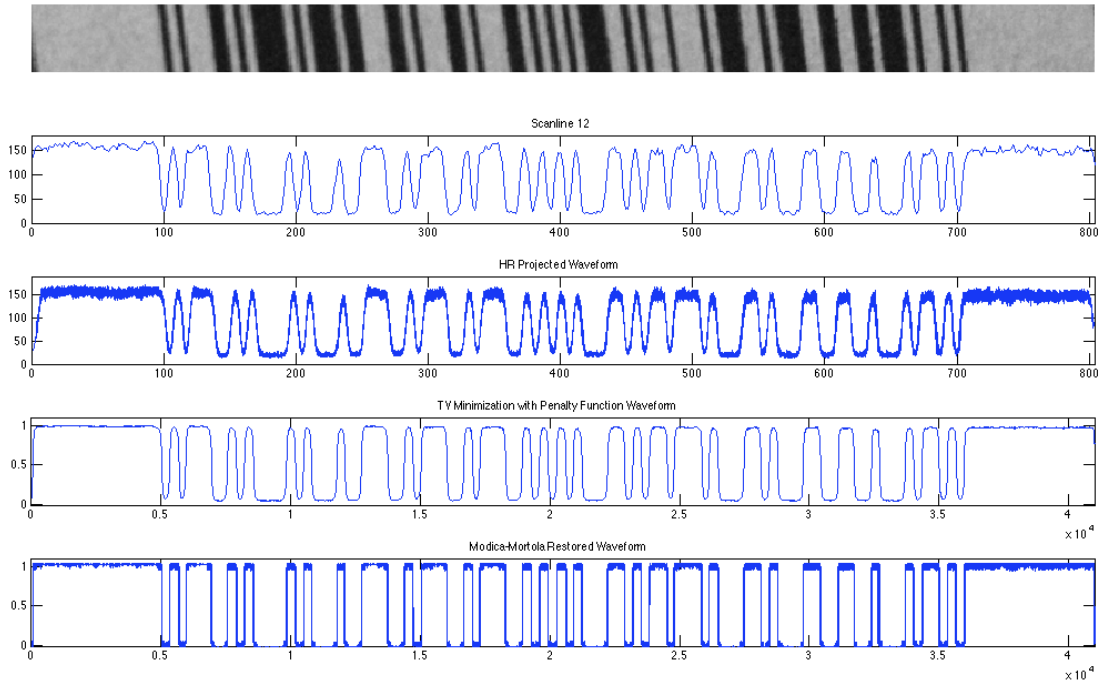

Figure 4.4: Real Roll Case
From top to bottom: Single Scanline, HR Projected Waveform, Modica-Mortola Restored Waveform($T = 5, \delta = \beta = \lambda = 0.1$), TV Restored Waveform ($T = 20, \delta = \beta = \lambda = 0.1$)

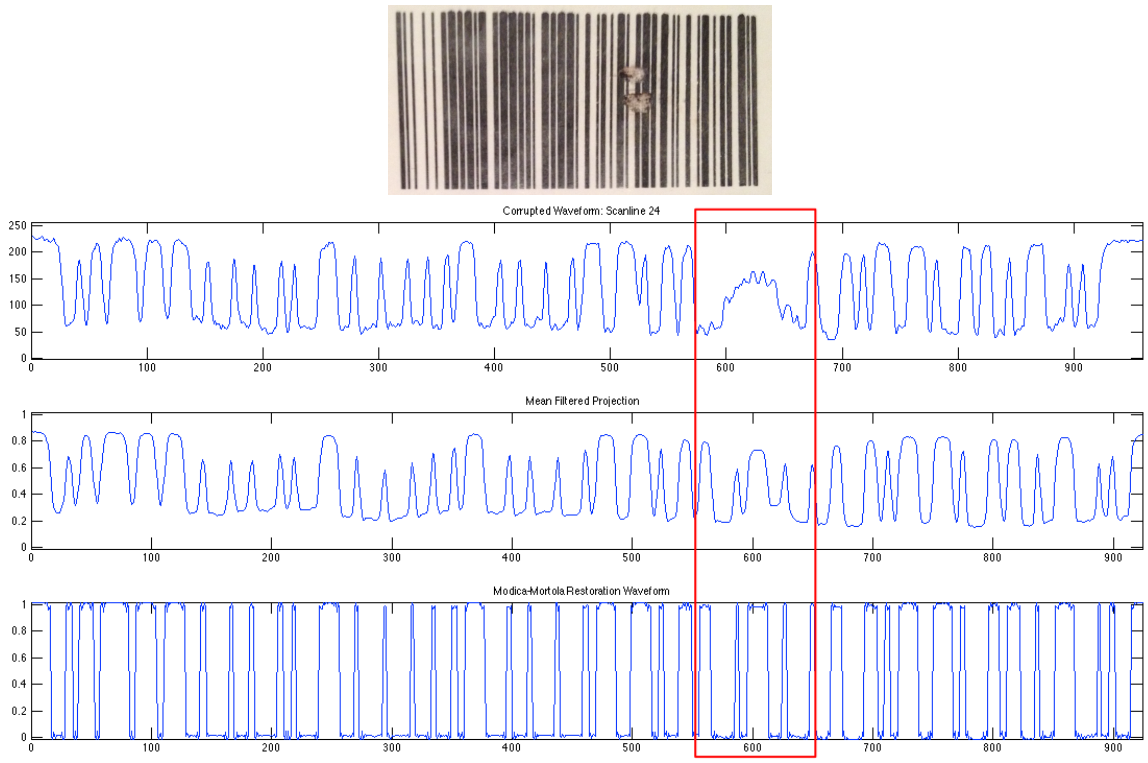

Figure 4.5: Locally Corrupted Barcode Image
From top to bottom: Corrupted barcode image, corrupted scanline waveform, mean filtered waveform, Modica-Mortola restored waveform $(T = 6, \delta = \beta = \lambda = 0.1)$.

4.4 Restoring Corrupted Images

The projection schemes and variational methods described in this paper are also useful for restoring a bilevel waveform from a corrupted barcode image. We present two examples of corrupted barcode images. The first has local corruption that affects only scanlines near the center of the image. The second shows universal corruption of the image that will prevent nearly all scanlines from decoding.

Figure 4.5 shows the first corrupted barcode image. The real image exhibits geometric sampling distortion, but for the illustration we assume that there is no rotation of the barcode within the plane of the image. An observed waveform is selected from the area of corruption. In the observed waveform, four bars are lost around $x = 600$. The mean filtered waveform

recovers these bars, and the Modica-Mortola algorithm restores the binary nature of the missing bars. There are multiple corrupted scanlines within this image that are not decodable by current decoding algorithms. However, without resampling of the image, the barcode can be decoded by application of the projection and variational method even in the presence of local corruption of the image data.

In practice, if a corrupted scanline is input into a decoding algorithm and fails to decode, a new scanline must be selected and the process repeated. However, if the input is instead a waveform created by the projection and restoration techniques described, the local corruption will not prevent decoding. This application can be extended to barcode images with multiple areas of local corruption and barcodes with universal corruption.

Figure 4.6 shows a barcode image with universal corruption. As in the previous example, geometric sampling distortion is evident, but for the illustration we make the same assumption of no rotation within the imaging plane. There is a line drawn through the barcode image. Nearly every scanline contains corruption that prevents the individual scanline from decoding. Three scanline waveforms are plotted in Figure 4.6 in order to show the effects of corruption. Localized corruption within individual scanlines is evident when comparing multiple scanlines extracted from the image. Scanline 15 is close to the top of the barcode image and consequently has corruption in the signal near $x = 2275$. Scanline 215 is extracted from the center of the image, and corruption can be seen near $x = 1300$. Scanline 415 is representative of a row of data near the bottom of the barcode image, and corruption is visible in the waveform near $x = 700$.

Applying a mean filter to the image shown in figure 4.6 and using the Modica-Mortola restoration scheme, we are able to recover the bilevel waveform from the corrupted image data. Figure 4.7 shows the mean filtered projection waveform and the Modica-Mortola restoration waveform. Each of the bars in the original barcode are restored.

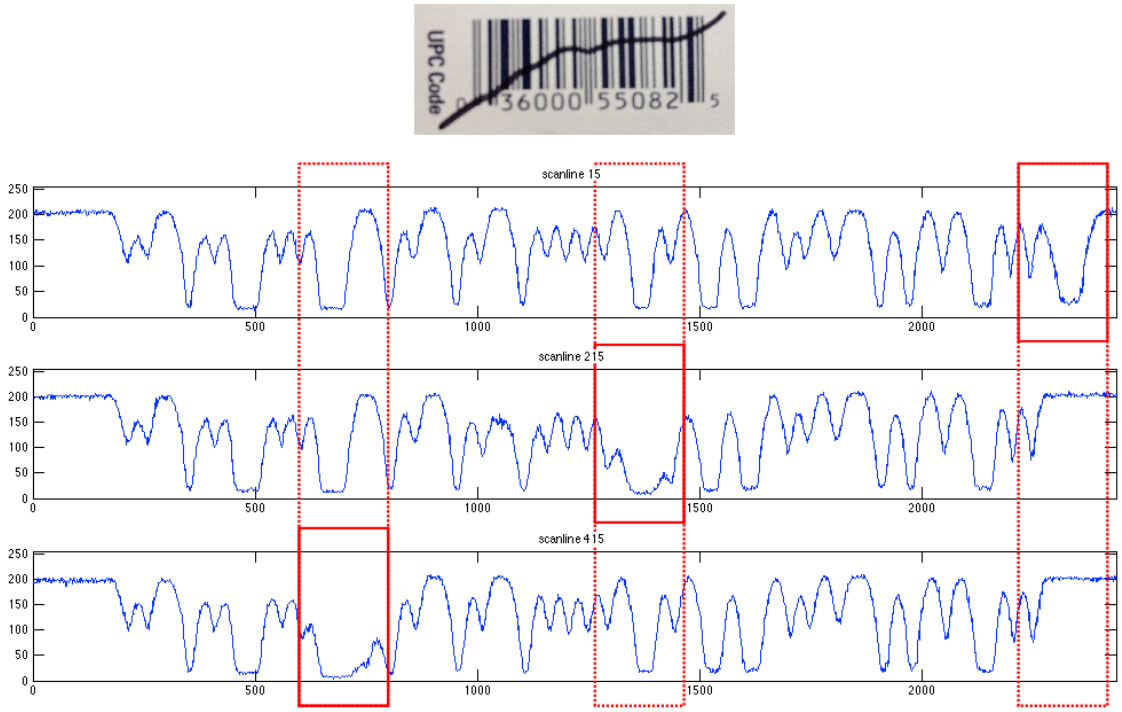

Figure 4.6: Universally Corrupted Barcode Image
From top to bottom: Observed scanline 15. Observed Scanline 215. Observed Scanline 415.

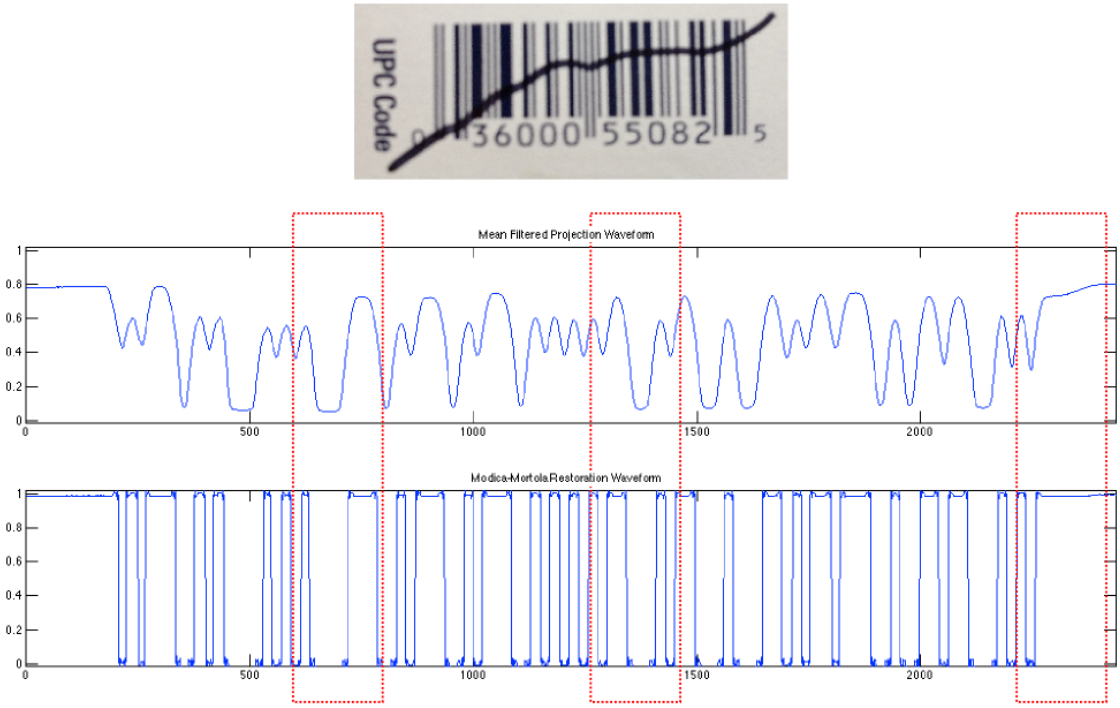

Figure 4.7: Restored Universally Corrupted Barcode Image
From top to bottom: Corrupted barcode image, mean filtered waveform, Modica-Mortola restoration waveform. $(T = 6, \delta = \beta = \lambda = 0.1)$.

Concluding Remarks

In this paper we have presented a series of modifications to well-known image processing algorithms in order to develop a variational approach for the restoration of bilevel waveforms from image data. We have adapted the concept of super-resolution of video in order to create a single waveform from the data contained in an image and applied restoration schemes to these waveforms for both synthetic and real initial data sets.

Many approaches to the super-resolution and restoration of bilevel waveforms have been previously addressed. A computer vision based method is employed by Oktem and Oktem [17]. Bailey created a phase image by Fourier Transforms in order to develop a super-resolution signal [6]. Esedoglu addresses deconvolution of waveforms by systematically estimating parameters [10].

This approach to bilevel waveform restoration is unique in that it extends the concept of super-resolution to the barcode restoration problem geometrically. We incorporate all of the data from an image when calculating the approximation of a single bilevel waveform. Our approach is noteworthy in the context of the application that we have chosen to elaborate on in this paper.

Our approach extends the concept of super-resolution of video to create a non-uniformly spaced waveform that combines all of the information present in the entire image. This waveform contains more information about the encoded binary sequence than we would be able to extract from a single uniformly spaced row of the pixelated barcode image.

We have addressed several synthetic and real barcode images that are not decodable by

current algorithms but are able to be decoded after the application of the methods described.

Further investigations may include sampling distortion generated from observing bar-codes on various topological spaces, numerical improvements to the techniques considered here, and other schemes for generating super-resolution signals.

Bibliography

Bibliography

[1] R. Acar and C.R. Vogel. Analysis of Total Variation penalty methods for ill-posed problems. *Inverse Problems*, 10:1217–1229, 1994.

[2] G. Alberti and C. Mantegazza. A note on the theory of SBV functions. *Boll. Un. Mat. Ital.*, B(7):375–382, 1997.

[3] L. Ambrosio. A compactness theorem for a new class of functions of bounded variation. *Boll. Un. Mat. Ital.*, B(7) 3:857–881, 1989.

[4] L. Ambrosio and V.M. Tortorellli. Approximation of functional depending on jumps by elliptic functionals via Γ-convergence. *Comm. Pure Appl. Math.*, 43:999–1036, 1990.

[5] G. Aubert and L. Vese. A variational method in image recovery. *SIAM J. Numer. Anal.*, 34:1948–1979, 1997.

[6] D. G. Bailey. Super-resolution of bar codes. *J. Electron. Imaging*, 10:204–213, 2001.

[7] T.F. Chan and J. Shen. *Image processing and analysis*. SIAM, Philadelphia, Pennsylvania, 2005.

[8] T.F. Chan and C. K. Wong. Total Variation blind deconvolution. *IEEE Trans. Image Process.*, 7:370–375, 1998.

[9] D.C. Dobson and F. Santosa. Recovery of blocky images from noisy and blurred data. *SIAM J. Appl. Math.*, 56:1181–1198, 1996.

[10] S. Esedoglu. Blind deconvolution of bar code signals. *Inverse Problems*, 20:121 ? 135, 2004.

[11] M. Irani and S. Peleg. Super resolution from image sequences. *ICPR*, 2:115–120, 1990.

[12] E. Joseph and T. Pavilidis. Deblurring of bilevel waveforms. *IEEE Trans. Image Process.*, 2:233–235, 1993.

[13] E. Joseph and T. Pavlidis. Bar code waveform recognition using peak locations. *IEEE Trans. Pattern Anal. Mach. Intell.*, 16:630–640, 1994.

[14] S. Osher L. Rudin and E. Fatemi. Nonlinear Total Variation based noise removal algorithms. *Phys. D*, 60:259–268, 1992.

[15] L. Modica and S. Mortola. Un esempio di Γ-convergenza. *Boll. Un. Mat. Ital.*, B 14:285–299, 1977.

[16] D. Mumford and J. Shah. Optimal approximations by piecewise smooth functions and associated variational problems. *Comm. Pure Appl. Math.*, 42:577–685, 1989.

[17] R. Oktem and L. Oktem. A superresolution approach for bar code reading. 2005.

[18] L. Rudin and S. Osher. Total Variation based image restoration with free local constraints. *In. Proc. 1st IEEE ICIP*, 1:31–35, 1994.

[19] M. K. Park S. C. Park and M. G. Kang. Super-resolution image reconstruction: a technical overview. *Signal Process. Mag., IEEE*, 3:21–26, 2003.

[20] M.I. Safran and R. Oktem. A fast Hough transform approximation and its application for barcode localization. *IEEE Signal Process. and Comm. Appl.*, pages 1–4, 2007.

[21] D. P. Goren S.J. Shellhammer and T. Pavlidis. Novel signal-processing techniques in bar code scanning. *IEEE Robot. Autom. Mag.*, March:57–65, 1999.

[22] S. H. Kang T.F. Chan and J. Shen. Total Variation denoising and enhancement of color images based on the cb and hsv color models. *J. Visual Comm. Image Rep.*, 12:422–435, 2001.

[23] L.A. Vese. A study in the BV space of a denoising-deblurring variational problem. *Appl. Math. Optim.*, 44:131–161, 2001.

[24] T. C. Wittman. *Variational approaches to digital image zooming*. PhD thesis, Univ. of Minn., 2006.

Appendix: MATLAB © Code

MATLAB © code used to implement the TV denoising scheme described in section 2.1.

```
function [u] = tv1(X, u0, epsilon, lambda)

% Total Variation (TV) Minimization
% Input: Original noisy waveform Y and x-coordinates X
% Output: TV denoised Waveform u

%Parameters
T = 20;     %Stopping time
dt = 0.1;   %Time step
a = 0.01;   %Fudge factor to avoid division by zero

u0 = double(u0);
u = u0;
m = length(u);

u_x=[];
u_xx=[];

for t = 0:dt:T
%Calculate derivatives
    u_x = u([2:m,m]) - u([1,1:m-1]);
    u_xx = u([2:m,m]) - 2*u + u([1,1:m-1]);
```

```
23
24      %TV term = Num/Den
25      Num = 2*(epsilon)*u_xx;
26      Den = (pi)*((epsilon).^2 + (u_x).^2)+a;
27
28      %Add to previous iteration of u.
29      u = u + dt*( Num./Den - 2*lambda*(u - u0));
30
31  end
```

MATLAB © code used to implement the TV denoising scheme with penalty function described in section 2.2.

```
function [u] = tv1dw(X, u0, epsilon, beta, lambda)

% Total Variation (TV) Minimization
% Input: Original noisy waveform u0, x-coordinates X, parameters ...
    epsilon, beta, and lambda
% Output: TV denoised Waveform u with values forced towards zero ...
    and one

%Parameters
T = 20;     %Stopping time
dt = 0.1;   %Time step
a = 0.01;   %Fudge factor to avoid division by zero.

u0 = double(u0);
u = u0;
m = length(u);

u_x=[];
u_xx=[];

for t = 0:dt:T

    u_x = u([2:m,m]) - u([1,1:m-1]);
    u_xx = u([2:m,m]) - 2*u + u([1,1:m-1]);

    %TV term = Num/Den
    Num = 2*(epsilon)*u_xx;
```

```
26      Den = (pi)*((epsilon).^2 + (u_x).^2)+a;
27
28      %Add to previous iteration of u.
29      u = u + dt*( Num./Den - 2*lambda*(u - ...
            u0)-beta*(2*u-6*u.^2+4*u.^3));
30
31  end
```

MATLAB © code used to implement the Modica-Mortola scheme described in section 2.4.

```
function [u] = MM(X, u0, epsilon, beta, lambda)

% Total Variation (TV) Minimization
% Input: Original noisy waveform u0, x-coordinates X, parameters ...
    epsilon, beta, and lambda
%        Parameter lambda (Try lambda=0.1)
% Output: TV denoised Waveform u

%Parameters
T = 1;     %Stopping time
dt = 0.1;  %Time step
a = 0.01;  %Fudge factor to avoid division by zero.

u0 = double(u0);
u = u0;
m = length(u);

u_x=[];
u_xx=[];

for t = 0:dt:T

    u_x = u([2:m,m]) - u([1,1:m-1]);
    u_xx = u([2:m,m]) - 2*u + u([1,1:m-1]);


    u = u + dt*( 2*a*u_xx - (1/epsilon)*(2*u - 6*u.^2 + 4*u.^3) -
```

```
27      2*lambda*(u-u0));
28  end
```

MATLAB © code used to implement the Projection scheme described in section 3.2.3.

```
function [ X, Y ] = projection( u0,theta )
%%Projects Roll Image onto a single ray of rotation to create a ...
    %%one-dimensinal signal.
%%u0 is the original image
%%theta is the known angle of rotation

S=size(u0);

if size(S,2)>2
u0=rgb2gray(u0);
end

X = [ ];
Y = [ ];
u=double(u0);
[m,n]=size(u0);
theta = theta * pi /180;
for y0=1:m
    for x0=1:n
       X = [X, x0*sec(theta) + ( (m-y0)-x0*tan(theta))*sin(theta)];
       Y = [Y , u(y0,x0)];
     end
end

[X,ind] = sort(X);
Y=Y(ind);


```

```
28
29 subplot(121);imshow(u0);title('Barcode Image');
30 subplot(122);
31 plot(X,Y);
32 title('Composite Scan Signal');
33
34 end
```